

# Brain Light-Tissue Interaction Modelling: Towards a non-invasive sensor for Traumatic Brain Injury

M. Roldan, S. Chatterjee, and P. A. Kyriacou, *Senior Member, IEEE*

**Abstract**— Traumatic brain injury (TBI) is one of the leading causes of death worldwide, yet there is no systematic approach to monitor TBI non-invasively. The main motivation of this work is to create new knowledge relating to light brain interaction using a Monte Carlo Model, which could aid in the development of non-invasive optical sensors for the continuous assessment of TBI. To this aim, a multilayer model tissue-model of adult human head was developed and explored at the near-infrared optical wavelength. Investigation reveals that maximum light (40-50%) is absorbed in the skull and the minimum light is absorbed in the subarachnoid space (0-1%). It was found that the absorbance of light decreases with increasing source-detector separation up to 3cm where light travels through the subarachnoid space, after which the absorbance increases with the increasing separation. Such information will be helpful towards the modelling of neurocritical brain tissue followed by the sensor development.

## I. INTRODUCTION

Traumatic brain injury (TBI) is, as its name indicates, an acquired head injury caused by an external force that disturbs the brain's function [1], [2]. TBI is among the most severe types of injury in terms of fatality and lifelong disability for survivors [3], [4]. Reported TBI incidence and mortality rates across the world vary considerably, yet there have been estimated 50 to 60 million new cases per year worldwide, of which over 80% occurred in low-middle income countries [5]. Nowadays, TBI assessment involves the use of non-continuous imaging techniques which are not always accessible, and invasive monitoring methods, encompassing the placement of a pressure transducer in the brain for monitoring intracranial pressure (ICP), one of the main biomarkers for assessing TBI. Such invasive techniques carry risks for the patient and require neurosurgical expertise for insertion. Both imaging and ICP monitoring involve potential delays before the information is available for clinical use [6] [7]. Furthermore, studies have shown that 60–80% of TBI patients go through an initial phase of cerebral hypoperfusion during the early post-traumatic period [7], contributing to increased mortality and a worse neurological outcome, especially if it cannot be assessed and treated on time [8]. Therefore, there is an unmet need in developing noninvasive techniques enabling the continuous monitoring of TBI, especially to assess brain's hemodynamic during the first hours after trauma, when secondary injury takes place [6].

\*There was no funding source for this study.

M. R. Author is with the Research Centre of Biomedical Engineering, City University of London, EC1V 0HB UK (corresponding author e-mail: maria.roldan@city.ac.uk).

Different types of near-infrared (NIR) spectroscopy systems and other multi-distance optical sensors have been developed since Jöbsis demonstrated that cerebral oxygen sufficiency can be monitored in vivo and non-invasively using NIR light [9]–[12]. Precise modelling of light propagation in the head to deduce the spatial sensitivity profile is crucial to the development and optimization of non-invasive optical technologies that aim to assess cerebral hemodynamic [13],[14]. The latter defines how deep the light travels into the tissue, where a large penetration depth carries to more accurate monitoring of the brain [13]. Also, the spatial sensitivity profile, so-called banana-shaped photon distribution, investigate the absolute absorption and scattering coefficients of the multiple tissue-layers of the head, which can be used to quantify chromophores' concentrations within the tissues [15].

Several theoretical and experimental studies have been performed to investigate the propagation of light in various head models, based on diffusion theory and Monte Carlo (MC) calculations. Except for a few studies, most approaches rely on homogeneous semi-infinite models of the head because of its simplicity [16]. However, the lack of realism might introduce bias in the measured optical properties [16]. In consequence, novel approaches based on heterogeneous structures have been considered [16]–[22]. These models consist of multiple layers, such as the scalp, the skull, cerebrospinal fluid (CSF) and the brain, which can be divided into grey and white matters. For instance, Okada et al. employed models consisting of three and four-layers to analyze photon propagation [23]. Although a few theoretical and experimental investigations on light propagation in the human head have been performed, knowledge of which layers in the brain are sampled by light at different source-detector distances remains incomplete. Such information is of the utmost importance to optimize the design and determine the sensitivity of the sensor.

In order to investigate the efficacy of an optical sensor to monitor the range of physiological changes related to TBI, the foremost step is to characterize the sensor on a healthy brain model. To this aim, in this work, a multilayered tissue model is developed and explored to analyze the optical interactions at the near-infrared wavelengths.

Dr. S. C. Author is with the Research Centre of Biomedical Engineering, City University of London, EC1V 0HB UK.

Dr. P.A.K. Author is with the Research Centre of Biomedical Engineering, City University of London, EC1V 0HB UK.

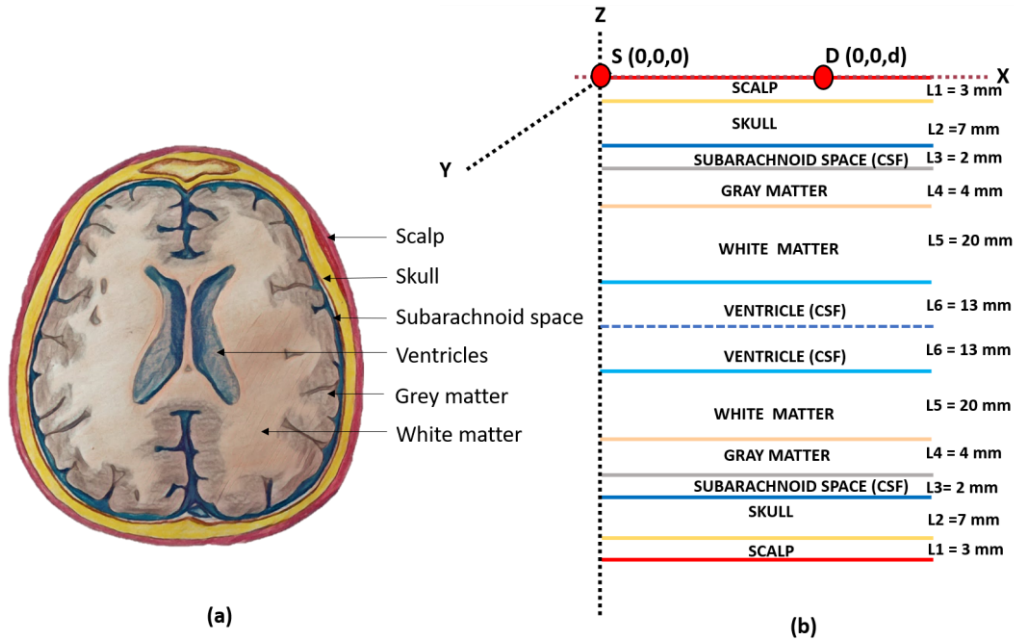


Fig. 1. Stratification of brain tissue layers: real (a) and simulated (b). The simulated tissue volume is presented in a 3D Cartesian co-ordinate system. A linear slab-geometry was chosen for the simulation due to simplicity.

## II. METHODS

The light-tissue interaction model simulated in this work used the Monte Carlo (MC) computational method. MC is a stochastic process to simulate the photon paths through a tissue volume based on the probabilities of scattering and absorption. The MC model has a range of proven advantages over other available modelling methods such as diffusion approximation, random walk theory or finite element method in terms of its straightforward approach, ability to incorporate random anisotropic scattering, inclusiveness of tissue heterogeneity and structural complexity, and flexibility regarding the sensor design and location [25]. Available MC models of brain-optics are either too complex and resource-consuming to replicate, or inadequately simplified. In the current work, a simple yet realistic multilayer brain-tissue model was developed and evaluated in a reflectance optical sensing geometry through a range the source-detection separations of 1, 2, 3 4 and 5 cm.

### A. Opto-anatomical parameters

The layer stratification of the Monte Carlo tissue-model is illustrated in Fig1. The full anatomical structure presented in Fig 1(a) was represented by a 12 layered semi-infinite slab-tissue model as shown in Fig 2(b) [31]. Healthy head layers thickness have been adopted from the literature as presented on Fig.1 [26], [27].

The tissue layers were characterized by their optical properties, namely, absorption coefficient ( $\mu_a$ ), scattering coefficient ( $\mu_s$ ), anisotropy function ( $g$ ) and refractive index ( $n$ ). The ideal wavelength for the sensor is the isosbestic point, i.e., 810nm since the absorption properties of the oxy- and

deoxyhemoglobin are the same at this wavelength, therefore, an optical signal independent of blood oxygenation can be recorded [24]. However, due to lack of adequate published information, the tissue-layer optical parameters through a near-infrared optical wavelength window (between 650-800nm) were adapted from literature and are illustrated in Table 1 [28].

Table 1 Optical coefficients of head tissues.

Layer	$\mu_a(mm^{-1})$	$\mu_s(mm^{-1})$	$g$	$n$
Scalp	0.016	19	0.9	1.60
Skull	0.018	16	0.9	1.56
Subarachnoid space	0.004	0.3	0.0	1.33
Grey matter	0.090	21.5	0.9	1.40
White matter	0.090	38.4	0.9	1.47
Ventricles	0.004	0.3	0.0	1.33

### B. Monte Carlo simulation strategy

The details of the MC simulation steps and algorithm are discussed in our previous publications [29], [30]. In the current work, a  $10^9$  number of photons were simulated through the brain tissue volume at each source-detector separation. Reflection loss at the air-tissue boundary and the interface between two tissue layers were considered in the model. In order to replicate a laser source, a Gaussian beam of a radius of 0.6mm was simulated. Photons were detected through a circular photodetector having an effective area of  $5mm^2$ .

The two simulated quantities discussed in this paper are - 1) layer-specific absorbance and 2) fractional optical pathlength. The absorbance and optical path through tissue are likely to vary with the sensor geometry according to the modified Beer-Lambert law [32]. Such information is important to optimize the source-detector separation for TBI

monitoring. The relative absorbance (presented in a percentage form) was calculated by recording the absorbance of each photon packet in each layer concerning the total absorbance of the photon packet within the entire head. Similarly, the fractional optical pathlength was calculated as the fraction of the pathlength of each photon concerning its total pathlength between the source and the detector. The absorbance and pathlength are the manifestations of the absorption and scattering properties of the tissue, respectively. Therefore, an analysis of both quantities leads to a comprehensive assessment of the sensor-tissue optical profile towards TBI investigation.

### III. RESULTS AND DISCUSSION

The Monte Carlo model investigated sensor-tissue optical profiles at the reflectance sensor geometry having source-detector separations 1-5cm at the near-infrared optical window are shown in Fig.2. The sampled thickness and width are presented at the y- and x-axes of the 2D projections of the 3D simulated distributions. The number density of the interaction events between the light and tissue are shown in the color bar. An accumulation of the interaction events is found near the source and the detector, and the number density decreases along with the depth interrogated by the sensor. Through the head tissue-layers, the interaction events are the lowest within the subarachnoid space (SAS) which has the lowest scattering coefficient and exhibits isotropic scattering ( $g = 0$ ), as shown in Table 1. The changes in the x-axes limit show the spatial distribution of light with the increasing source-detector separation, for example, the spatial distribution of light at 1cm and 4cm separations are about 20mm and 45mm, respectively. The mean depth of penetration at  $d = 1, 2, 3, 4$  and 5cm separation distances are about 6mm (scalp), 8mm (skull), 11mm (subarachnoid space), 13mm (grey matter) and 15mm (white matter).

The relative absorbance at each tissue layer is shown in Fig. 3. Utilizing the current sensor design, the maximum tissue-layer that can be interrogated is grey matter. The

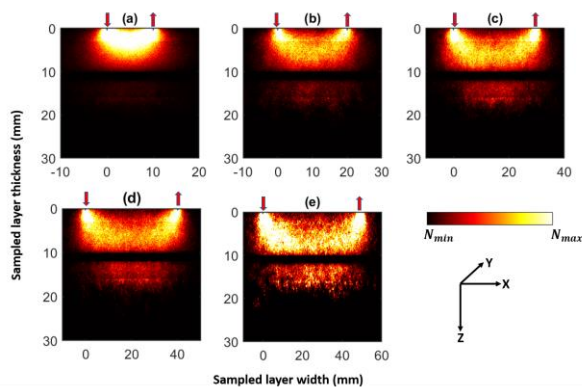


Fig. 2. Monte Carlo simulated photon path through normal brain tissue at different source-detector separations: 10, 20, 30, 40 and 50mm as shown in (a), (b), (c), (d), and (e), respectively. The x- and y-axis represent the sampled width and thickness of the tissue volume. The downward and upward arrows are the locations of the source and the detector, respectively. The y-axes are presented in the same scale. The x-axes scales are different due to the semi-infinite width of the simulated tissue volume. The color bar represents the distribution of the number of photon-tissue interactions (N) between its minimum and maximum values

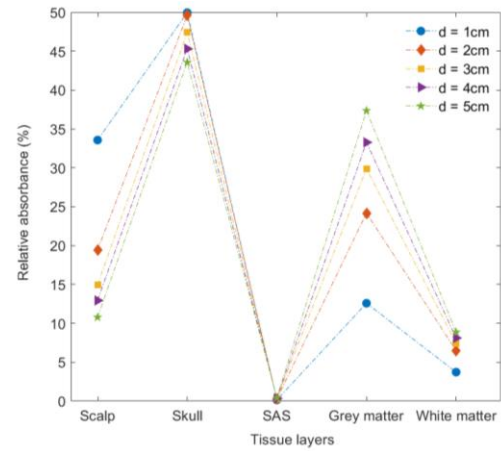


Fig. 3. Relative absorbance at different head tissue layers at the source-detector separations  $d = 1, 2, 3, 4$  & 5cm. The absorbance of the head tissue layers scalp, skull, subarachnoid space (SAS), grey matter and white matter are presented. No photons could reach beyond the white matter, so rest of the simulated tissue layers are not shown. The maximum and minimum relative absorbances are shown in the skull and subarachnoid spaces, respectively.

maximum and minimum absorbances are found in the skull and the subarachnoid space, respectively, at all source-detector separations. Interestingly, at the superficial tissue layers such as scalp and skull, the relative absorbance decreases with the increasing source-detector separations whereas, at the deeper layers such as grey and white matter, the reverse incident takes place. This is a combined effect of the sensor geometry and the optical wavelength that will be helpful to assess brain tissue with less interference of extracerebral tissues, especially at source-detector distances above 3cm.

The fractional optical pathlength at different tissue layers are presented in Table 2. Optical pathlength depends on (a) the scattering coefficient and (b) the number of photons scattered in the tissue layer. The highest fractional optical pathlength at skull is the result of the maximum photon scatter density at this layer as shown in Fig.2. Even though the scattering coefficients of the grey and white matter are relatively high, the numbers of photon scatter at these tissue layers are lesser since a fewer number of photons can penetrate to this depth. The fractional optical pathlength information is invaluable to calculate the differential pathlength factors of the tissue at the TBI sensor geometry to quantify the tissue perfusion [33].

Table 2 Simulated fractional optical path at different tissue layers at source-detector separations  $d = 1-5$ cm.

$d$ (cm)	Fractional optical pathlength				
	Scalp	Skull	Subarachnoid space	Grey matter	White matter
1	0.41	0.54	0.01	0.027	0.008
2	0.28	0.63	0.014	0.061	0.016
3	0.23	0.65	0.017	0.082	0.020
4	0.21	0.64	0.022	0.095	0.023
5	0.18	0.65	0.0278	0.112	0.023

One of the key aspects to carry out the present Monte Carlo simulation was to determine the source-detector separation for the TBI sensor. From the investigation, it is inferred that with a source-detector separation as high as 5cm, light can interrogate through white matter and no light reaches the ventricles. Several serious TBI conditions including hemorrhage (subdural, epidural, subarachnoid and intracerebral) and edema (vasogenic and cytotoxic) are mostly found within or around the tissue layers such as the subarachnoid space, grey matter and white matter which can be accessed utilizing one of the simulated sensor geometries.

### Conclusion

A robust yet simplistic Monte Carlo model of multilayered human head has been developed enabling the comprehensive investigation of light tissue interaction of adult brain. The findings demonstrate clearly the potential of non-invasive optical sensors in TBI. Such sensors could enable the non-invasive monitoring of some of the most prominent TBI biomarkers such as intracranial pressure and/or cerebral oxygenation. Future work will aim to model, using Monte Carlo techniques, the physiological changes associated with TBI and to determine the sensitivity of the proposed sensor to those changes. The simulated information could then be implemented into the sensor design for TBI patient monitoring.

### REFERENCES

[1] B. I. A. of America, "ABI vs. TBI: What is the difference?," 2021. [Online]. Available: <https://www.biausa.org/brain-injury/about-brain-injury/nbiic/what-is-the-difference-between-an-acquired-brain-injury-and-a-traumatic-brain-injury>. [Accessed: 08-Jan-2021].

[2] Headway, "Types of brain injury | Headway," 08-Jan-2021. [Online]. Available: <https://www.headway.org.uk/about-brain-injury/individuals/types-of-brain-injury/>. [Accessed: 08-Jan-2021].

[3] A. Brazinova *et al.*, "Epidemiology of Traumatic Brain Injury in Europe: A Living Systematic Review," *J. Neurotrauma*, Dec. 2018.

[4] B. D. Greenwald, D. M. Burnett, and M. A. Miller, "Congenital and Acquired Brain Injury. 1. Brain Injury: Epidemiology and Pathophysiology," *Arch Phys Med Rehabil*, vol. 84, no. 1, 2003.

[5] A. I. R. Maas *et al.*, "Traumatic brain injury: integrated approaches to improve prevention, clinical care, and research," *Lancet Neurol.*, vol. 16, no. 12, pp. 987–1048, 2017.

[6] M. Martin *et al.*, "Prediction of Early Intracranial Hypertension After Severe Traumatic Brain Injury: A Prospective Study," *World Neurosurg.*, vol. 127, pp. e1242–e1248, 2019.

[7] C. Sokoloff *et al.*, "Clinical Usefulness of Transcranial Doppler as a Screening Tool for Early Cerebral Hypoxic Episodes in Patients with Moderate and Severe Traumatic Brain Injury," *Neurocrit. Care*, 2019.

[8] A. T. Mazzeo and D. Gupta, "Monitoring the injured brain," *J. Neurosurg. Sci.*, vol. 62, no. 5, pp. 549–562, 2018.

[9] F. F. Jöbsis, "Noninvasive, infrared monitoring of cerebral and myocardial oxygen sufficiency and circulatory parameters," *Science (80-. )*, vol. 198, no. 4323, pp. 1264–1266, 1977.

[10] M. Roldan, T. Y. Abay, and P. A. Kyriacou, "Non-invasive techniques for multimodal monitoring in Traumatic Brain Injury (TBI): systematic review and meta-analysis," *J. Neurotrauma*, p. neu.2020.7266, Aug. 2020.

[11] M. N. Kim *et al.*, "Continuous Optical Monitoring of Cerebral Hemodynamics During Head-of-Bed Manipulation in Brain-Injured Adults," 2014.

[12] W. Weigl *et al.*, "Application of optical methods in the monitoring of traumatic brain injury: A review," *Journal of Cerebral Blood Flow and Metabolism*, vol. 36, no. 11. Nature

Publishing Group, pp. 1825–1843, 01-Nov-2016.

[13] J. K. Choi, J. M. Kim, G. Hwang, J. Yang, M. G. Choi, and H. M. Bae, "Time-Divided Spread-Spectrum Code-Based 400 fW-Detectable Multichannel fNIRS IC for Portable Functional Brain Imaging," *IEEE J. Solid-State Circuits*, vol. 51, no. 2, pp. 484–495, Feb. 2016.

[14] T. Li, Y. Li, Y. Sun, M. Duan, and L. Peng, "Effect of head model on Monte Carlo modeling of spatial sensitivity distribution for functional near-infrared spectroscopy," *J. Innov. Opt. Health Sci.*, vol. 8, no. 5, p. 8, Sep. 2015.

[15] J. Selb, T. M. Ogden, J. Dubb, Q. Fang, and D. A. Boas, "Comparison of a layered slab and an atlas head model for Monte Carlo fitting of time-domain near-infrared spectroscopy data of the adult head," *J. Biomed. Opt.*, vol. 19, no. 1, p. 016010, 2014.

[16] M. Dehaes *et al.*, "Assessment of the frequency-domain multi-distance method to evaluate the brain optical properties: Monte Carlo simulations from neonate to adult," *Biomed. Opt. Express*, vol. 2, no. 3, p. 552, 2011.

[17] T. Li, H. Gong, and Q. Luo, "Visualization of light propagation in visible Chinese human head for functional near-infrared spectroscopy," *J. Biomed. Opt.*, vol. 16, no. 4, p. 045001, 2011.

[18] S. Mahmoodkalayeh and M. A. Ansari, "A subject-specific layered head model for monte carlo fitting in time-domain near-infrared spectroscopy," *Proc. - Int. Conf. Laser Opt. 2018, ICLO 2018*, vol. 19, p. 518, 2018.

[19] R. Mudra, A. Nadler, E. Keller, and P. Niederer, "Analysis of near-infrared spectroscopy and indocyanine green dye dilution with Monte Carlo simulation of light propagation in the adult brain," *J. Biomed. Opt.*, vol. 11, no. 4, p. 044009, 2006.

[20] L. Wu, Y. Lin, and T. Li, "Effect of Human Brain Edema on Light Propagation: A Monte Carlo Modeling Based on the Visible Chinese Human Dataset," *IEEE Photonics J.*, vol. 9, no. 5, 2017.

[21] Q. Zhang, E. N. Brown, and G. E. Strangman, "Adaptive filtering for global interference cancellation and real-time recovery of evoked brain activity: a Monte Carlo simulation study," *J. Biomed. Opt.*, vol. 12, no. 4, p. 044014, 2007.

[22] Y. Zhang, J. W. Sun, and P. Rolfe, "RLS adaptive filtering for physiological interference reduction in NIRS brain activity measurement: A Monte Carlo study," *Physiol. Meas.*, vol. 33, no. 6, pp. 925–942, Jun. 2012.

[23] E. Okada, M. Firbank, M. Schweiger, S. R. Arridge, M. Cope, and D. T. Delpy, "Theoretical and experimental investigation of near-infrared light propagation in a model of the adult head," *J. Appl. Opt.*, vol. 36, no. 1, p. 21, 1997.

[24] J. M. Murkin and M. Arango, "Near-infrared spectroscopy as an index of brain and tissue oxygenation," *Br. J. Anaesth.*, vol. 103, no. SUPPL.1, pp. i3–i13, 2009.

[25] S. Chatterjee and P. A. Kyriacou, "Monte carlo analysis of optical interactions in reflectance and transmittance finger photoplethysmography," *Sensors (Switzerland)*, vol. 19, no. 4, Feb. 2019.

[26] K. U. Maheswari and S. Sathiyamoorthy, "Soft tissue optical property extraction for carcinoma cell detection in diffuse optical tomography system under boundary element condition," *Optik (Stuttg.)*, vol. 127, no. 3, pp. 1281–1290, Feb. 2016.

[27] L. Ragan, I. Waczulikova, L. Guller, J. Bilicky, and J. Benuska, "Cella media distance in human brain in relation to age and gender," *Biomed. Pap.*, vol. 153, no. 4, pp. 307–313, 2009.

[28] F. B. Haeussinger, S. Heinzl, T. Hahn, M. Scheckmann, A. C. Ehlis, and A. J. Fallgatter, "Simulation of near-infrared light absorption considering individual head and prefrontal cortex anatomy: Implications for optical neuroimaging," *PLoS One*, vol. 6, no. 10, Oct. 2011.

[29] K. Budidha and P. A. Kyriacou, "Investigating the origin of photoplethysmography using a multiwavelength monte carlo model," *Physiol. Meas.*, vol. 41, no. 8, p. 084001, Sep. 2020.

[30] S. Chatterjee, J. P. Phillips, and P. A. Kyriacou, "Monte Carlo investigation of the effect of blood volume and oxygen saturation on optical path in reflectance pulse oximetry," *Biomed. Phys. Eng. Express*, vol. 2, no. 6, p. 065018, Dec. 2016.

[31] Wang, L., Jacques, S.L. and Zheng, L., 1995. MCML—Monte Carlo modeling of light transport in multi-layered tissues. *Computer methods and programs in biomedicine*, 47(2), pp.131-146.

- [32] Chatterjee, S., Budidha, K. and Kyriacou, P.A., 2020. Investigating the origin of photoplethysmography using a multiwavelength Monte Carlo model. *Physiological Measurement*, 41(8), p.084001.
- [33] Chatterjee, S., Abay, T.Y., Phillips, J.P. and Kyriacou, P.A., 2018. Investigating optical path and differential pathlength factor in reflectance photoplethysmography for the assessment of perfusion. *Journal of biomedical optics*, 23(7), p.075005.